Dual-Wetting Porous Plate System to Measure Drainage and Imbibition Capillary Pressure: A Case Study on a Complex Reservoir Carbonate

Franck Nono[1*], Titly Farhana Faisal[1], Nacer Benlalam[2], Isabelle Jolivet[1], Clément Varloteaux[3], Mohamed Regaieg[1], Georgy Borisochev[3], Abbas Zerkoune[1], and Cyril Caubit[1]

[1]TotalEnergies, CSTFJ, Avenue Larribau, 64000 Pau, France
[2]Polytechnic of Turin, Italy
[3]Computational Hydrocarbon Laboratory for Optimized Energy Efficiency, 64000 Pau, France

Abstract. Capillary pressures data are essential for understanding the initial fluid distribution in reservoirs prior to production (Primary drainage) or for predicting oil recovery during waterflooding processes (first imbibition). Coupled with Digital Rock Physics tools, these properties also provide valuable pore-scale insights into rock's topology and wettability distribution within the pore network. Recent studies [1, 2] have demonstrated the predictivity of pore network multiphase flow simulations when accurate pore-scale wettability observations are performed, on simple and permeable rocks. Trying to understand different wettability patterns becomes even more important when dealing with complex rocks where a significant amount of porosity is below the resolution of 3D images. This paper introduces a dual-wetting porous plate system designed to measure both drainage and imbibition capillary pressure curves on the same rock, under constant experimental conditions, including wettability alteration. The PEEK cell is X-ray transparent, enabling 3D saturation monitoring via micro-CT, and is adaptable to SCAL protocols. Validation was performed on a 20mD complex carbonate reservoir rock, including wettability alteration with crude oil. Primary drainage and first imbibition capillary pressure curves were first both derived numerically with a conventional Unsteady State relative permeability experiment on a large sample. In a second time, we used a mini plug from the same SCAL sample's depth, to derive primary drainage and imbibition capillary pressure curves with our dual-wetting porous plate system, under identical experimental conditions than the SCAL experiment. The results showed good agreement between the SCAL and our DRP experiments, confirming the proof of concept of the system. Additionally, 3D images processing of the mini plug enabled observation of the sequence of invasion of different porosity textures, providing insights into wettability distribution. This experimental design offers valuable input for understanding the impact of wettability patterns on multiphase flow properties.

1 Introduction

Recent developments [1, 2, 3] in Digital Rock Physics (DRP) have markedly improved the accuracy and efficiency of relative permeability computations, particularly by addressing the complex issue of wettability distribution within pore network models. Innovative DRP wettability experiments now provide detailed insights into how wettability varies with pore size and the proportion of water-wet versus oil-wet pores. These experiments are termed "Amott-like" because they follow the procedural framework of conventional Amott tests.

Currently, the DRP predictive workflow is most effective for permeable rocks where over 85% of the porosity can be resolved using 3D X-ray imaging. This high-resolution imaging threshold is essential for visualizing and quantifying fluid saturation within the pore space, thereby limiting the applicability of this method to rocks with sufficiently high porosity resolution.

In more complex lithologies, unresolved porosity, pore spaces below the imaging resolution threshold, can represent a significant fraction of total porosity. While fluid content in these regions can be estimated using differential imaging or histogram normalization [4, 5], direct visualization of fluids and wettability distribution at this scale remains unattainable with standard micro-CT techniques.

The Amott-like DRP experiment is structured around two spontaneous and two forced phases, being only punctual steps of a complete capillary pressure cycle. For complex rocks, it is necessary to collect intermediate data throughout the entire capillary pressure cycle, including both drainage and imbibition phases, to better constrain wettability interpretation in unresolved porosity. Water-wet primary drainage capillary pressure data elucidate the structure and connectivity of the pore network, while imbibition capillary pressure provides further insight into wettability distribution across both visible and invisible pore networks. Ideally, the full capillary pressure cycle should be performed on the same sample, as using

* Corresponding author: franck.nono@totalenergies.com

different samples for drainage and imbibition increases variability and complicates data reconciliation, especially when dealing with heterogeneous small samples size.

Capillary pressure curves are typically measured in laboratories using established petrophysical methods, including centrifuge (CF), porous plate (PP), and mercury injection (MICP). In general, MICP is achieved only under primary drainage (imbibition MICP considered not reliable), whereas PP and CF are applied to both drainage and imbibition experiments. Unlike MICP, CF and PP techniques allow the use of crude oil, thereby incorporating reservoir wettability into the capillary pressure curves and making them more robust for imbibition measurements. However, CF generally does not permit measurement of the positive part of the imbibition curve, while PP does, albeit with greater time requirements.

Despite their technical maturity, the direct application of CF and PP techniques to measure full drainage and imbibition capillary pressure curve on DRP samples remains limited due to the sensitivity of DRP samples to disturbances during experiments. Maintaining consistent experimental conditions throughout the full capillary pressure cycle is particularly challenging, and in this way conventional CF and PP setups are difficult to put in place.

Alternative approaches, such as the semi-dynamic methodology [6], derive capillary pressure curves by analyzing inlet saturation and pressure gradients across the plug during various injection rates. While this method minimizes experimental disturbances, it does not provide sufficient statistical data to characterize wettability distribution across the entire pore network.

Over the past two to three decades, new devices have been developed to enable direct measurement of both drainage and imbibition capillary pressure curves on the same sample. For example, Longeron et al. [7] designed a cell with a changeable semi-permeable membrane, but this approach is prone to incomplete membrane saturation, disturbance of capillary equilibrium during membrane replacement, and lack of saturation profile monitoring. Later, Fleury et al. [8] integrated two semi-permeable membranes into a single cell, successfully measuring both drainage and imbibition on preserved samples. However, this design also presented drawbacks such as for example: (i) increased risk of gas introduction during loading and unloading of semi-permeable membranes because the sample is saturated without the membranes, (ii) potential system plugging when using crude oil, and (iii) the inability to measure flow properties such as permeability with the membranes in place.

More recently, Victor et al. [9] introduced a single T-shaped water-wet porous plate design that allows switching between capillary pressure establishment and flow property assessment. While this innovation enables fast and robust primary drainage achievement, it does not support both drainage and imbibition measurements without altering experimental conditions.

In summary, measuring the complete capillary pressure cycle, including water-wet primary drainage, wettability alteration under controlled conditions, saturation monitoring, imbibition experiments and flow property assessment remains a significant technical challenge. Obtaining the full capillary pressure cycle with additional flow properties measurement is crucial for understanding wettability, which is a key parameter in predicting reservoir fluid dynamics through DRP approaches. Accurate characterization of wettability at the pore scale is essential, as the predictive capability of pore network modeling tools depends on a detailed understanding of wettability distribution within the rock.

This study introduces an innovative experimental setup featuring two T-shaped porous plates, one water-wet and one oil-wet, integrated within the same system. The accompanying protocol enables the complete capillary pressure cycle to be measured under rigorously controlled conditions. Throughout the experiment, both confining and pore pressures are maintained constant, ensuring stable experimental parameters. The ageing process is conducted without any modification to the system, with the sample held at maximum primary drainage capillary pressure and periodic refreshing of crude oil as required. Additionally, effective permeabilities are determined at residual saturations, including 100% brine saturation, $S_{wi,}$ and S_{orw}. The cell is also designed to facilitate three-dimensional imaging of the entire sample at each stage of the capillary pressure cycle.

To validate the proposed concept, a complex reservoir carbonate rock was subjected to a complete capillary pressure cycle measurement utilizing the newly developed design. The resulting capillary pressure data were systematically compared with SCAL data obtained from a larger sample extracted at the same depth.

2 Materials and methods

2.1 Dual porous plate design and methodology

The dual porous plate system utilized in this study is depicted in Fig. 1. Dual porous plate system. Valves 1 and 4 enable viscous flooding while valves 2 and 3 enable porous plate measurement.. The design is based on the configuration described by Victor et al. [9], employing the same T-shaped porous plate and cell system. However, in contrast to the original setup, which featured a single bottom porous plate, the present design incorporates two porous plates: one positioned at the bottom and another at the top of the sample.

Both porous plates are fabricated from alumina (Al_2O_3) and are initially supplied in a water-wet state. A key advantage of this configuration is the ability to bypass the porous plate system, enabling viscous flooding through the sample and allowing for direct measurement of the pressure gradient across the core. To modify the wettability of the plates, the protocol described by Lewis et al. [10] was applied, converting selected water-wet plates to an oil-wet state. It is possible to use initially oil-wet plates. The final assembly consists of a water-wet porous plate at the bottom and an oil-wet porous plate at the top of the sample.

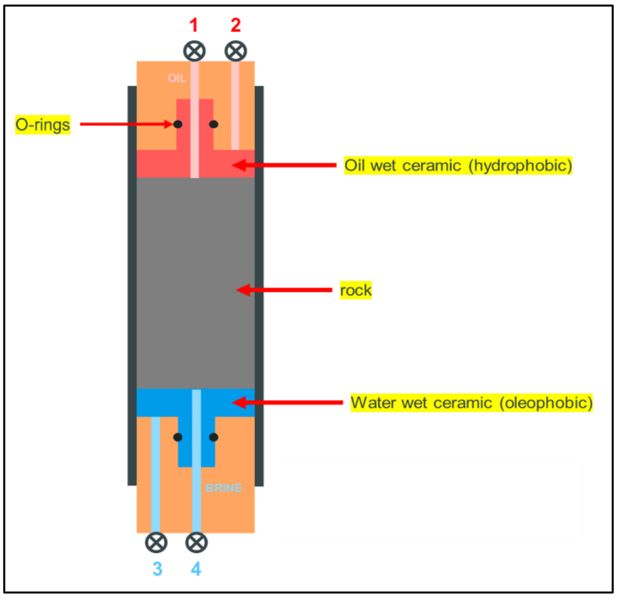

Fig. 1. Dual porous plate system. Valves 1 and 4 enable viscous flooding while valves 2 and 3 enable porous plate measurement.

Additionally, grooves were machined into the surface of each porous plate in contact with the sample. This modification, as referenced by Nono et al. [11], is intended to minimize flow disturbances near the end-faces of the sample during viscous flooding operations.
The porous plates and sample are initially assembled in a dry state. The entire system, including the top oil-wet porous plate, is then fully saturated with brine under confining pressure. This initial configuration ensures hydraulic continuity between the brine in the rock and the brine in the bottom water-wet porous plate up to valve 3, enabling accurate measurement of primary drainage and positive imbibition capillary pressure curves.
Primary drainage and positive capillary pressure experiments can then be conducted by injecting or retrieving oil from valve 1, resulting in the displacement of brine from the sample to valve 3. Following these steps, oil may be present in valve 4 due to prior oil flooding operations, such as effective permeability measurements at S_{wi}.
Before commencing the negative imbibition capillary pressure measurement, it is necessary to re-establish brine continuity from valve 4 to the bottom face of the sample. This is achieved by injecting multiple pore volumes of brine from valve 3 to valve 4 with valves 1 and 2 closed, thereby displacing oil from the bottom tubings and ensuring brine saturation, as illustrated in Fig. *2*, step (1): Cleaning brine arrival.
The negative imbibition capillary pressure step also requires continuity of the oil phase from the sample to the top valve 2, and such continuity is not initially present since the system is fully saturated with brine.

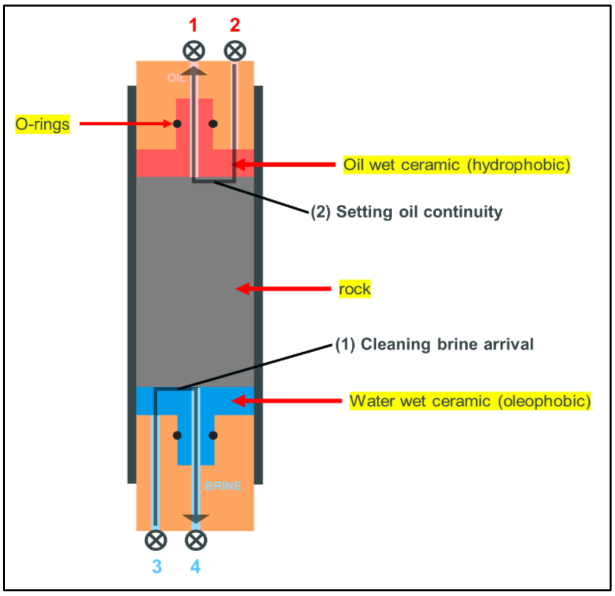

Fig. 2. Setting continuity of phases during full cycle capillary pressure measurements: (1) cleaning brine arrival and (2) setting oil continuity, both to start negative Pc imbibition step.

To avoid dismantling the system and compromising experimental conditions, oil continuity is established by injecting oil from valve 2 to valve 1, with valves 3 and 4 closed. The flooding direction is depicted in Fig. *2*, step (2): Setting oil continuity. During this process, the oil-wet porous plate, initially saturated with brine, is oil-flooded. This step theoretically leaves disconnected brine clusters within the porous plate while maintaining oil connectivity. After no more brine is produced and the dead volumes are totally filled with oil, continuity is achieved from the sample to valve 2, with minimal disturbance to the sample's saturation, as the system remains near zero capillary pressure.
Once this step is complete, the negative imbibition capillary pressure experiment can proceed by injecting brine from valve 4, which will displace oil towards valve 2.

2.2 Porous media

The reservoir rock-type used in this study is a carbonate sample consisting of more than 99% calcite, with a grain density of 2.71 kg/dm3. MICP tests were conducted on plugs extracted from the upper and lower sections of the investigated interval. These tests revealed a dominant pore-throat size peak at approximately 1 µm, with a significant portion of the porosity interconnected by throats ranging from 4 µm down to 0.2 µm in radius (see

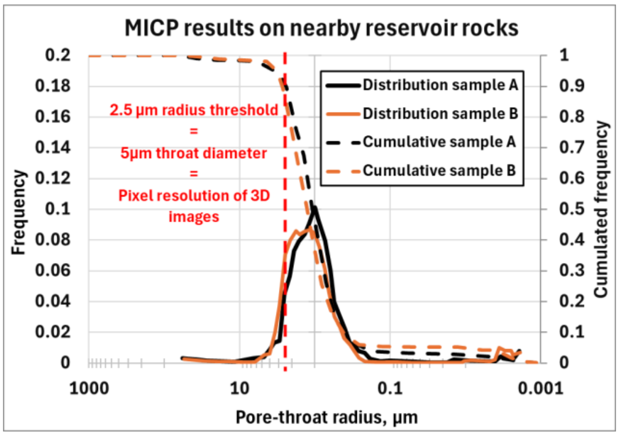

Fig. *3*).

For the experimental work, two samples drilled at the same depth were selected. The first is a homogeneous SCAL cylindrical plug, measuring 5 cm in diameter and 13.8 cm in length, which was used for an unsteady-state relative permeability experiment. The second sample is a mini plug, 1 cm in diameter and 14 mm in length, employed in our newly designed dual porous plate DRP cell to capture the complete capillary pressure cycle.

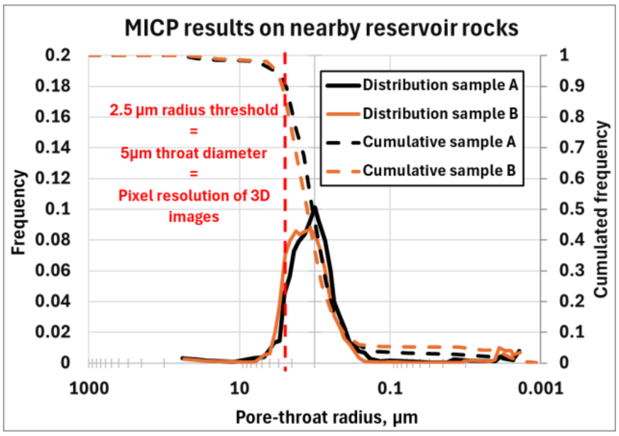

Fig. 3. MICP results of two samples A and B were taken near the samples investigated in this study.

All tests (SCAL and DRP) were conducted under identical experimental conditions, including the same confining and pore pressures and identical fluid types. Both samples display comparable porosities and absolute permeabilities (see Table 1).

Table 1. Petrophysical properties of reservoir rocks used in this study

	D (cm)	L (cm)	ϕ (p.u.)	K_w (mD)	$S_{wi,}$ (s.u.)
SCAL	5	13.8	27.5 +/-0.6	25 +/- 5	8.8
DRP	1	1.4	29.5+/-1	19.2 +/- 4	7.2

Permeability measurements for both samples were performed under 100% brine-saturated conditions by applying a minimum of eight different flow rates. Pressure gradients across the samples were accurately recorded using Rosemount® pressure sensors, and absolute permeability values were calculated using the one-phase flow Darcy equation. The final uncertainty in permeability was determined by accounting for devices precision, sample geometry, and brine properties.

2.2.1 Mini Plug for DRP Dual porous-plate experiment

Absolute permeability of the mini plug was determined through direct experimental measurement, while average porosity and porosity profiles were derived exclusively from 3D image processing utilizing a differential imaging approach [4]. Cross-sectional illustrations of the mini plug are presented in Fig. *4*.

The mini plug exhibited an absolute permeability of 19.2 +/- 4 mD and an average total porosity of 29.5 +/- 1 p.u. Of this, 22 p.u. (approximately 75% of the total) is attributed to unresolved porosity, while 7.3 p.u. is accounted for by resolved porosity. An example of illustration of the unresolved porosity regions is shown in Fig. *5*. Porosity profiles, shown in Fig. *6*, indicate some variability and suggest the presence of slightly heterogeneous zones within the sample. Visual inspection (see Fig. *4*) further reveals potential differences in pore structure between the upper and lower halves of the mini plug. Using 3D image segmentation and internal pore network extraction algorithms, as commonly applied in our DRP workflows [12], we analyzed the resolved pore size distributions of both halves. The comparison, illustrated in Fig. *7*, demonstrates a slightly greater prevalence of larger pores in the lower half compared to the upper half of the sample.

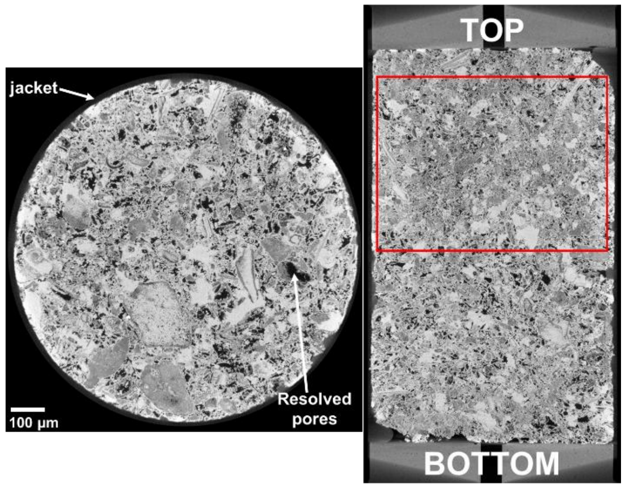

Fig. 4. Transversal (left) and longitudinal (right) cross-sections of the mini plug. The red zone will be the focus of wettability comparisons with SCAL experiment.

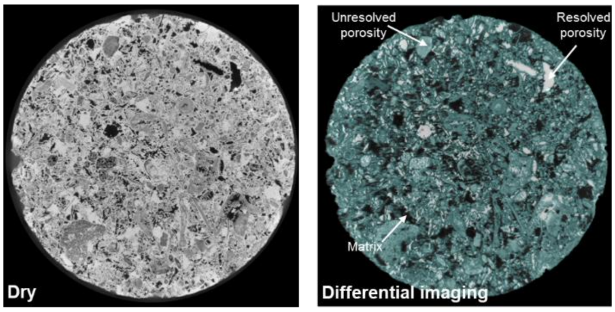

Fig. 5. Left – dry section of the mini plug, Right – result from differential imaging with green color representing the unresolved porosity.

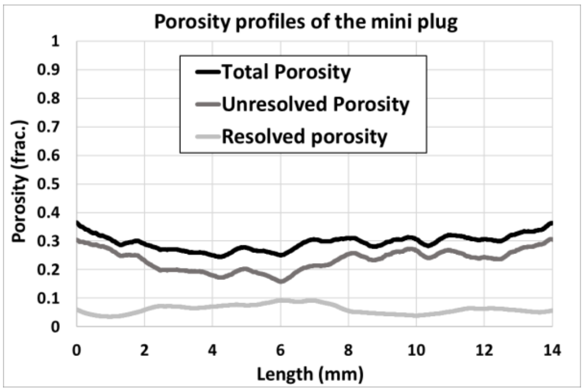

Fig. 6. Porosity profiles of the mini plug determined through 3D image processing

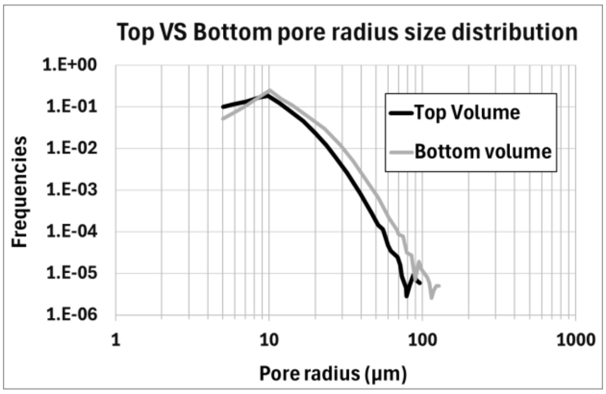

Fig. 7. Pore size distribution comparisons between a top and a bottom identical volume of the mini plug.

2.2.2 SCAL plug for Unsteady-State Kr experiment

The SCAL plug has a diameter of 5 cm and a length of 14 cm. The measured absolute permeability is 25+/-5 mD, and the porosity under experimental conditions (net confining pressure) is 27.5+/-0.6 p.u (see Table 1). Dispersion tests were conducted to assess the homogeneity of the plug along the flow direction. Two tests were performed, alternating between formation brine and the same brine diluted by a factor of four. The dispersion flow rate (1.5 pore volumes per hour) was sufficiently high to minimize diffusive effects and highlight any heterogeneities present in the flow direction. The resulting normalized concentration curves, plotted against pore volumes injected, are shown in Fig. ***8***.

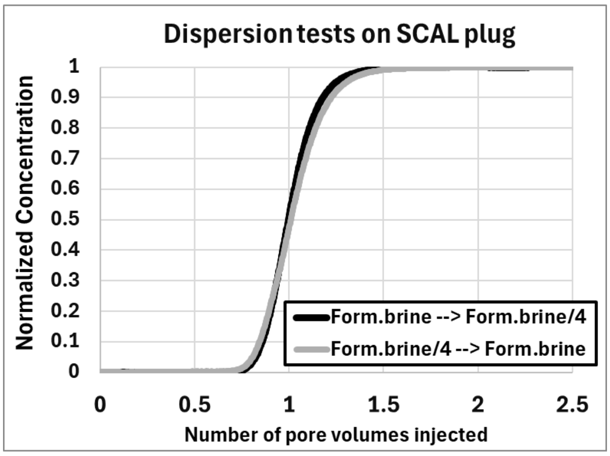

Fig. 8. Dispersion tests results on the SCAL reservoir plug.

Results suggest that the sample is uniform and homogeneous in the direction of fluid flow.

2.3 Fluids

In this study, we focus on two phase flow (oil/brine) displacements. For this initial proof of concept, it was essential to maintain identical experimental conditions across all tests to eliminate variability in results attributable to procedural differences. In microtomography, fluid doping is required to enhance contrast between phases and facilitate image processing. Accordingly, the brine used in both the SCAL and DRP experiments was an adapted formation brine, supplemented with sodium iodide as a dopant (see **Table *2***).

Table 2. Adapted formation brine composition

Salts	Concentration (g/l)
NaCl	71
NaI	100
KCl	14.4
$MgCl_2 + 6H_2O$	6
$CaCl_2 + 6H_2O$	19

Primary drainage in both experiments (SCAL and DRP) was conducted using Marcol52 (M52).
For the ageing process, crude oil sourced from the reservoir was employed to modify wettability. Following ageing, crude oil was replaced with mineral oil prior to the imbibition phase, in both experiments. This substitution was necessary due to limitations in the DRP experimental setup, which cannot accommodate high-temperature micro-CT operations.
During imbibition, a lighter mineral oil (IsoparL) was used. The primary objective was to prevent disturbances such as viscous fingering during SCAL unsteady state waterflooding. IsoparL was selected for its viscosity, which closely matches that of brine under experimental

conditions (30°C), thereby promoting stable displacement during SCAL waterflooding.
In summary, both experiments were designed to account for their respective limitations and minimize artefacts. A summary of the fluids and their properties is provided in Table 3.

Table 3. Fluids properties used in this study

Fluids	T (°C)	ρ (g/cc)	μ (cP)
Marcol52 (M52)	20	0.84	10.7
Adapted F. brine		1.14	1.2
Crude Oil	80	0.83	2.9
IsoparL	30	0.77	1.13
Adapted F. brine		1.1	0.95

Solely, for the differential imaging approach, the mini plug sample is first saturated with a 300 g/l sodium iodide brine to provide a high contrast full brine 3D image to better locate the sub-porosity regions using differential imaging technique.

2.4 Images acquisition and processing

Three-dimensional X-ray images of the mini plug were acquired using the Zeiss Versa 520 microtomograph. The imaging parameters were set to an energy of 90 kV and a power of 8 W, with a voxel size of 5 µm. The system's 2000x2000 pixel camera enabled full coverage of the sample diameter (10 mm) in a single scan. However, to capture the entire sample length (14 mm), two overlapping segments were acquired and subsequently stitched together using dedicated 3D reconstruction software, resulting in a global 3D volume of the mini plug.
Image processing was performed using ImageJ software. For general flooding steps, the adapted formation brine (see Table 3) was primarily used. As a result, differential imaging could not be applied for saturation tracking within the sub-resolved porosity during these steps. Instead, we used the histogram's peak approach explained in [5] where two additional sets of 3D images are acquired: one with the sample fully saturated with mineral oil, and another fully saturated with the adapted formation brine. Saturation changes within the sub-resolved porosity are then quantified by applying a linear interpolation of the histogram peak corresponding to the sub-resolved porosity, between its maximum value (100% formation brine) and minimum value (100% mineral oil), following image normalization.

3 Experiments

3.1 Unsteady-state relative permeabilities (SCAL)

A primary drainage unsteady-state relative permeability experiment is conducted by injecting mineral oil (M52) at progressively increasing flow rates into the SCAL plug initially fully saturated with the adapted formation brine. Throughout the injection process, pressure gradient, the produced volumes, and saturation profiles as a function of time were systematically recorded. The initial injection flowrate was carefully selected to prevent unstable displacement and to enable the acquisition of multiple transient saturation profiles prior to breakthrough. These transient profiles, in conjunction with the equilibrium saturation profiles, were used to further constrain the numerical inversion and reduce uncertainties in the determination of reliable couples Kr/Pc curves.
To facilitate the search of global maxima during numerical inversion, particularly for the accurate determination of capillary pressure curve points, the initial estimates were based on the semi-dynamic methodology, which posits that the equilibrium pressure gradient is equivalent to the capillary pressure at the entry. The use of our in-situ saturation monitoring device [13] provided direct visualization of entry saturation, allowing for the acquisition of pressure gradient versus entry S_w data points. Upon reaching the targeted initial water saturation, a reverse flow was applied to homogenize the saturation profile, after which the effective oil permeability at S_{wi} was measured.

Subsequently, the mineral oil was replaced with crude oil, and the system was aged at 80 °C under quasi-static flow conditions for one month, during which ten pore volumes of crude oil were injected. The crude oil was periodically refreshed throughout the ageing period, and between refreshing cycles, it was maintained static at pore pressure.

Following the ageing process, the crude oil was replaced with mineral oil (IsoparL). The effective oil permeability was measured post-ageing, and a first imbibition experiment was performed by injecting brine at incrementally increasing flowrates. As in the primary drainage step, the initial flow rate was set very low to prevent unstable displacement and to allow for the acquisition of multiple transient saturation profiles prior to breakthrough. During waterflooding, the pressure gradients, the produced oil volumes, and saturation profiles were recorded. Bump rates were applied at the end of the experiment to approach residual oil saturation. Finally, the effective permeability to brine was measured.

3.2 Full cycle of capillary pressure (DRP)

Prior to initiating the primary drainage capillary pressure experiment, the absolute permeability of the mini plug is measured. Primary drainage is then performed by injecting mineral oil (M52) from the top of the sample towards the bottom water-wet porous plate, with the inlet oil pressure progressively increased in steps. At each pressure increment, once equilibrium is achieved, defined as the time by which no further oil injection occurred, a three-dimensional X-ray scan of the entire sample is conducted. When S_{wi} is reached, the effective permeability to oil is measured. Subsequently, the mineral oil is then replaced with crude oil at 80 °C, ensuring that the replacement pressure gradient remains

below the final capillary pressure value recorded during primary drainage.
The ageing phase lasted one month, during which 10 pore volumes of crude oil are injected to refresh the oil within the sample. Between each refreshment, the maximum capillary pressure obtained during primary drainage is maintained.
Following the ageing period, the crude oil is replaced with mineral oil (IsoparL), and the effective oil permeability at S_{wi} is measured. The positive and negative imbibition processes are then conducted according to the methodology described in Section 2.1. Upon completion of the negative imbibition experiment, the effective permeability to brine is determined.

4 Results and discussions

4.1 SCAL Unsteady State Kr experimental results

4.1.1 Primary drainage

Numerical inversion on experimental results to determine relative permeability (Kr) and capillary pressure (Pc) curves was performed using the commercial **Cydar®** software.

For the primary drainage experiment, oil was injected while brine production, pressure gradient, and saturation profiles were monitored until reaching S_{wi}. The experimental and inversion results are shown in Fig. *9*. The observed saturation profiles display a clear positive gradient towards the outlet, which is consistent with a water-wet system and confirms the effectiveness of our flow-through cleaning protocol [5].

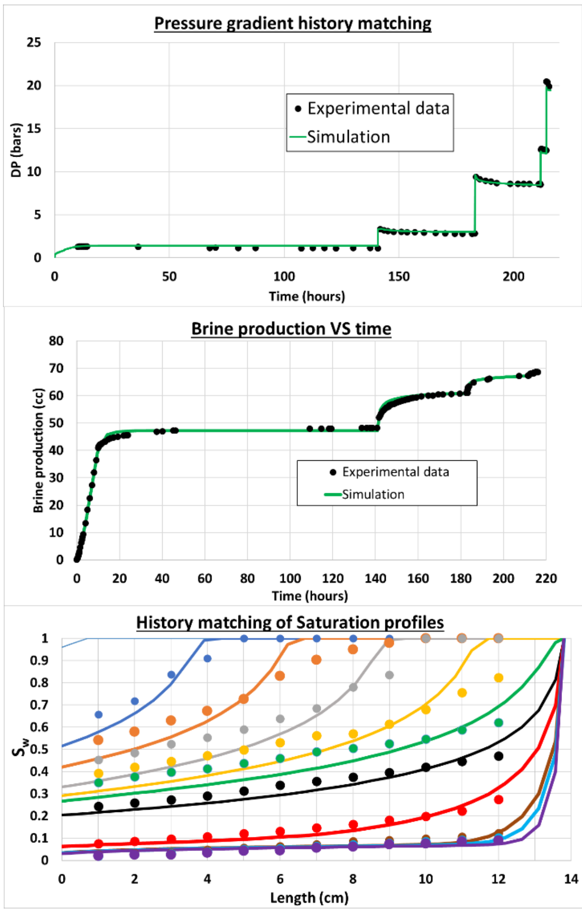

Fig. 9. Experimental and inversion results for the primary drainage unsteady state experiment.

For the numerical inversion on the saturation profiles, experimental data from a few centimeters at both the top and bottom of the sample were systematically excluded due to the presence of steel diffusers, which reduce the signal-to-noise ratio near the end faces of the sample. In addition, the final saturation profile after flow reversal was intentionally not included in the inversion to simplify the convergence. Overall, the agreement between the experimental data and the numerical results is excellent.
The derived Kr and Pc curves are presented in Fig. *10*. As expected, the final Pc results closely match the initial $Pc(S_w)$ first guess to run the inversion. The Corey exponents used to characterize the primary drainage relative permeability curves are provided in Table 4.

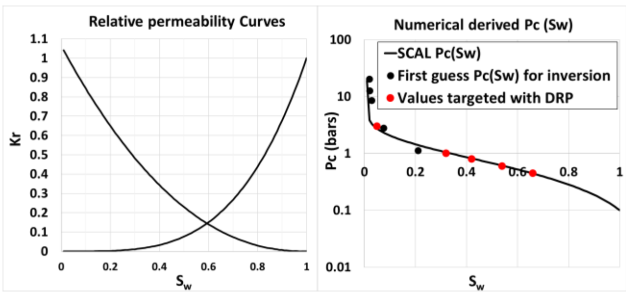

Fig. 10. Kr (linear) and Pc (log) results from the numerical inversion. On Pc graphics (right), the red dots will be the target of the Dual porous plate experiment

4.1.2 First imbibition

Following the same workflow applied to the primary drainage experiment, Kr and Pc were obtained through numerical inversion of the experimental dataset, including oil-production curve, pressure-gradient evolution, and both transient and equilibrium saturation profiles acquired at each imposed brine flowrate. The experimental observations and corresponding history-matching results are presented in Fig. ***11***.

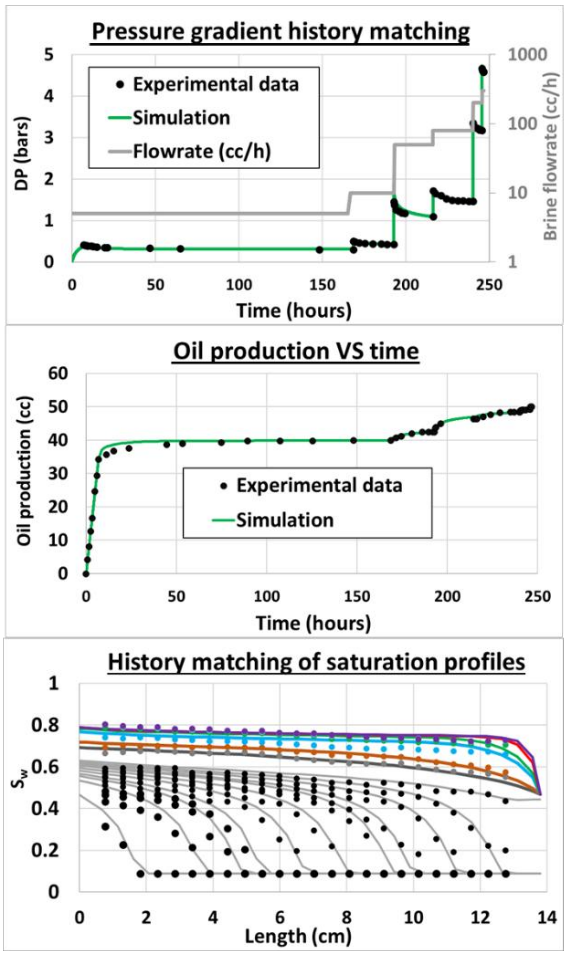

Fig. 11. Experimental and inversion results for the first imbibition unsteady state experiment

An increase in oil production with increasing brine flow rate is clearly observed, together with a negative saturation gradient towards the outlet end of the sample. These trends confirm that the wettability of the sample shifted following the ageing procedure. The quality of history matches, particularly the agreement with transient saturation profiles is good.

The final $P_c(S_w)$ and $K_r(S_w)$ curves derived from the inversion are shown in Fig. ***12***, while the fitted parameters are summarized in Table 4. SCAL measurements were conducted prior to the DRP experiments, as the resulting capillary pressure curves provided an initial basis for selecting an appropriate saturation range and corresponding capillary pressure targets for the dual porous-plate setup. Fig. ***10*** and Fig. ***12*** include, in red, the P_c VS S_w porous plate target points derived from these SCAL capillary pressure results.

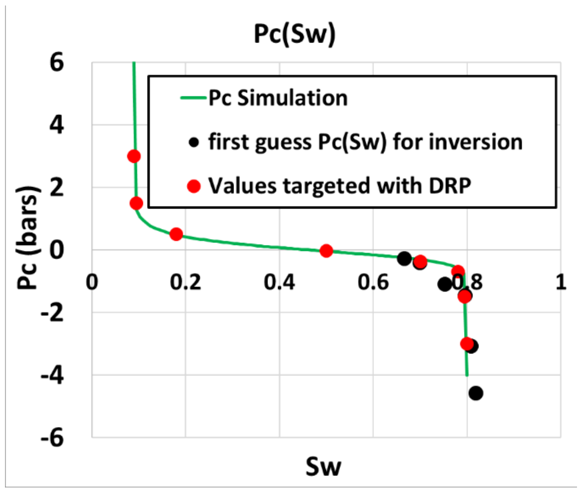

Fig. 12. Kr and Pc results from the numerical inversion. On Pc graphic, the red dots will be the target of the Dual porous plate experiment

Table 4. Fitting parameters of relative permeabilities obtained through numerical inversion of SCAL primary drainage and first imbibition experiments

Primary drainage					
n_w	n_o	$K_{rw,\,max}$	$K_{ro,\,max}$	$S_{wi\ exp.}$	$S_{wi\ simu.}$
3.66	2.21	1	1.04	0.08	0.01

First imbibition							
n_w	n_o	$K_{rw,\,max}$	$K_{ro,\,max}$	$S_{wi\ exp.}$	S_{wi} simu.	S_{orw}	S_w @ Pc=0
5.4	3.3	0.77	0.91	0.08	0.08	0.2	0.46

4.2 DRP Dual porous plate experimental results

4.2.1 Primary drainage

Saturation profiles acquired at each capillary pressure VS saturation equilibrium are presented in Fig. ***13***. Capillary pressure was imposed using a pump that maintained a constant pressure gradient across the mini-plug and the water-wet porous plate; under these conditions, the applied pressure gradient is equal to the capillary pressure. A Rosemount® pressure sensor, with an uncertainty of ±5 mbar, ensured accurate regulation of the imposed pressure. Once mineral-oil injection was halted, brine production ceased, and a three-dimensional image of the sample was recorded.

The saturation profiles exhibit a clear contrast between the top of the sample (farthest from the outlet) and the bottom, consistent with visual observations and the pore-size distribution analysis discussed in Section 2.2.

The final average irreducible water saturation, S_{wi} = 7.2 s.u., is in close agreement with the 8 s.u. measured from SCAL experiments.

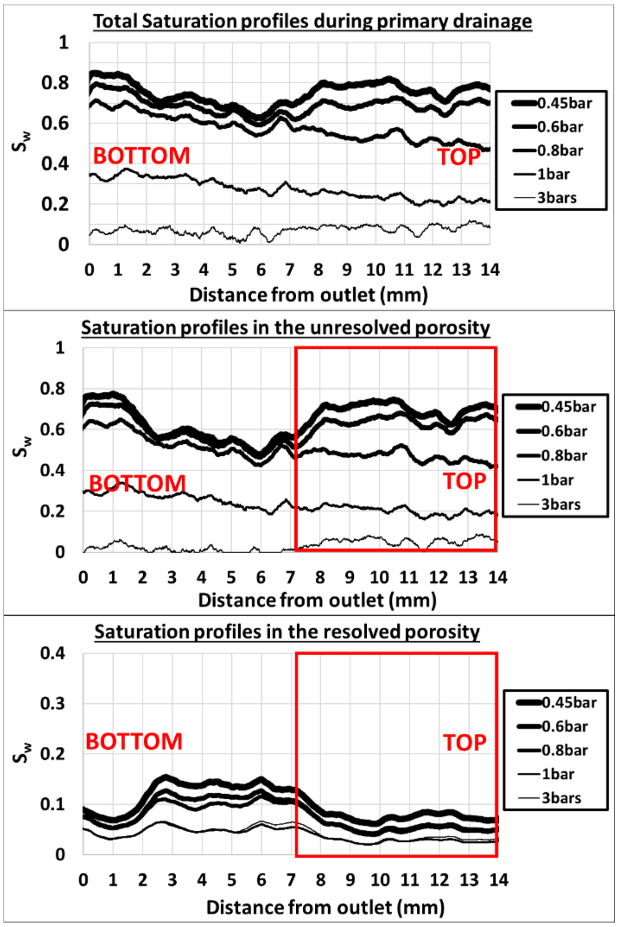

Fig. 13. Saturation profiles of porous plate primary drainage, from top to bottom: Top - Total saturation profiles, Middle - in the unresolved porosity, Bottom - in the resolved porosity. Red box indicates top homogeneous zone.

Comparisons of the capillary pressure curves obtained from the dual porous-plate primary drainage experiment show excellent agreement with the numerically derived SCAL Pc functions, as illustrated in Fig. *14*.

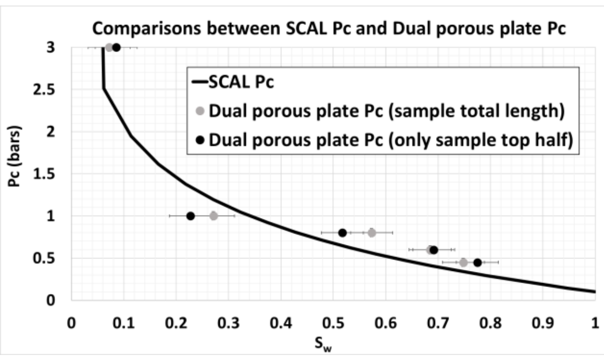

Fig. 14. Primary drainage capillary pressure vs saturation results comparisons between the SCAL and Dual porous plate experiments. An uncertainty of +/- 4 s.u. is generally ascribed to image processing.

4.2.2. First imbibition (positive and negative)

During positive capillary pressure stage, oil pressure is decreased stepwise, and a 3D image is acquired at each step. For the negative capillary pressure stage, brine pressure is increased incrementally to reach the final target values. Because of wettability alteration and limits of our microfluidic system, injected brine volume variations were not always clearly detectable from the pump level. To ensure consistent acquisition, each step is therefore held for one week before imaging, introducing some uncertainty in the true equilibrium brine saturation, which might therefore be slightly higher than the measured values as full capillary equilibrium may not be achieved.

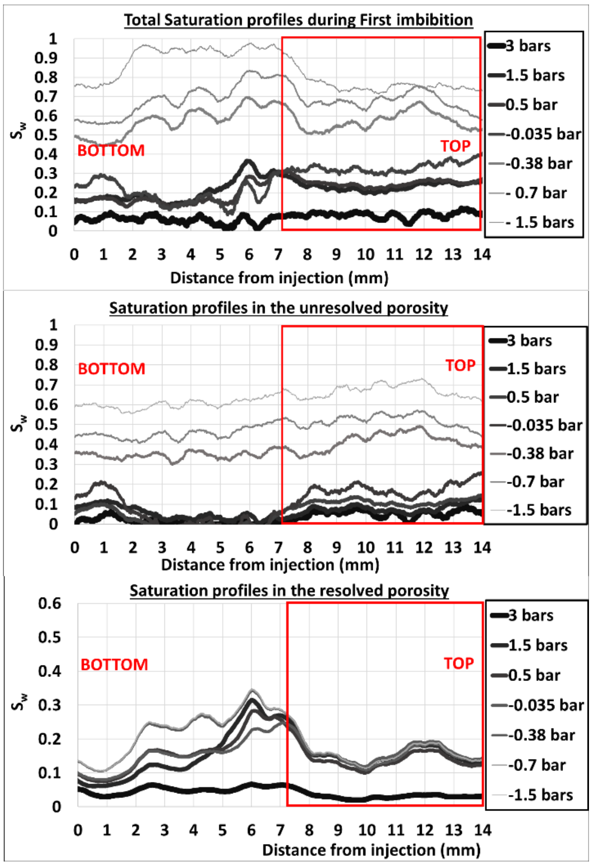

Fig. 15. Saturation profiles of dual porous plate system during first imbibition, from top graphic to bottom graphic: Total saturation profiles, unresolved saturation profiles and resolved saturation profiles. Red box indicates top homogeneous zone.

The final equilibrium saturation profiles (Fig. *15*) reveal distinct behaviors at the injection (bottom) and outlet (top) ends. The top half (red box in Fig. *15*) spans a narrower saturation range with final values close from that of the SCAL experiment, whereas the bottom half reaches $S_w \approx 0.95$ with only 5 s.u. of residual oil. In contrast, the minimum residual oil in the top half is ROS = 22 s.u. In the resolved-porosity domain, saturation in the top half remains nearly constant above Swi, while slight variations appear in the bottom half. In the unresolved-porosity domain, brine does not enter the bottom half during the positive Pc stage but does invade the top half. Under negative Pc, brine fills the bottom half and continues to invade the top unresolved domain. These results indicate that, during spontaneous imbibition, brine preferentially invades the resolved porosity in the bottom half and the unresolved porosity in the top half. Under forced imbibition, brine desaturates the unresolved porosity in both regions. Plots of Pc versus average S_w for the dual porous-plate imbibition experiment (Fig. ***16***) show that the top-half behavior aligns well with the SCAL Pc curves. Because the top half is more homogeneous and exhibits end-point saturation values consistent with the SCAL data, it was selected for the wettability distribution assessment.

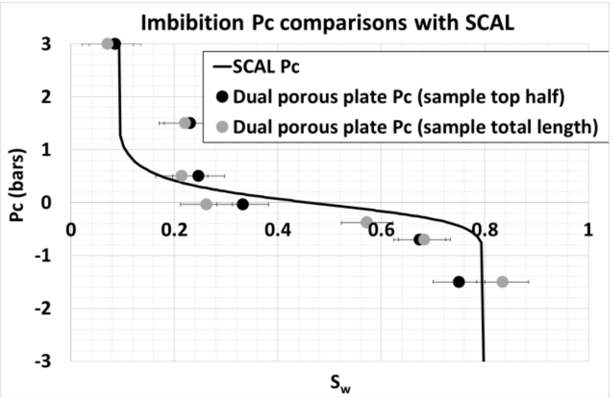

Fig. 16. First imbibition capillary pressure vs saturation results comparisons between the SCAL and Dual porous plate experiments. An uncertainty of +/- 4 s.u. is generally ascribed to image processing.

4.3 Pore-scale wettability distribution

A key strength of the dual porous plate design is that it combines a complete capillary pressure cycle with 3D imaging at each Pc step, allowing saturation changes to be tracked independently within different porosity textures. In this section, this capability is used to follow fluid invasion across throat-size regions, especially within the unresolved porosity. The interpretation follows the two stages of the experiment: primary drainage is used to identify dominant throat-size regions and their spatial distribution, while subsequent waterflooding tracks saturation changes within these same regions to reveal their wettability-dependent response during imbibition.

This distinction is critical for complex carbonate such as the rock studied in this study, where about 75% of the porosity remains unresolved and cannot be characterized using resolved-pore wettability methods [1,2].

In the case of resolved porosity, wettability interpretation is relatively straightforward, as pore sizes are explicitly known and can be directly linked to saturation occupancy. By contrast, the main challenge arises in the unresolved porosity, where pore sizes span a continuous spectrum that cannot be explicitly visualized. In this domain, the difficulty is to determine where within the unresolved pore space different wettability responses arise, and how these can be isolated in a physically meaningful way. Addressing this challenge is essential if pore scale observations are to be translated into inputs suitable for pore network modelling. For this reason, the interpretation presented in this section focuses on the unresolved porosity. The analysis presented below is restricted to the top half of the mini plug (red box highlighted in Figure 4, Figure 13 and Figure 15), which corresponds to the more homogeneous zone identified in Section 2.2 and exhibits the closest agreement with the SCAL reference capillary pressure curves.

4.3.1 Unresolved porosity: throat-size subregion discrimination

Before the primary drainage, all pores are initially water-wet. Under these conditions, oil invasion follows an invasion percolation regime governed by throat size, with pores connected to the largest accessible throats drained first at the lowest applied Pc. Saturation maps (where each unresolved porosity voxel has saturation between $0<S_w<1$) are generated using the 3D tomography images acquired at each drainage Pc step. Voxels that exhibit a sharp saturation drop higher than 50% saturation change between two consecutive Pc steps are indicative of pores connected to relatively narrow throat-size populations draining simultaneously, whereas voxels showing more progressive saturation changes across several steps reflect broader throat-size distributions and gradual drainage. In this study, 50% threshold was found to be the best compromise that enables a real focus on regions that clearly exhibit a clear change while keeping on track a non-negligible amount of the total porosity. Below, the main information starts to be diluted and above, the volume of investigation starts to be negligible.

Using the Young–Laplace relationship (see equation 1) together with the measured oil–brine interfacial properties, each imposed drainage capillary pressure step can be associated with a characteristic range of throat sizes that are preferentially invaded at that pressure.

$$P_c = \frac{2.\gamma.Cos(\theta_r)}{r} \quad (1)$$

Where Pc is the capillary pressure, γ is the interfacial tension, Θ_r is the receding contact angle and r is the throat radius. The measured IFT of the couple of fluids oil/brine used in this study is 40 $mN.m^{-1}$ and the receding contact angle value used to derive throat sizes is $\Theta_r = 25°$ with a standard deviation of 5°. These values are generally used to simulate primary drainage in our predictive DRP Kr simulations studies presented in [1,2].

For the five drainage Pc steps applied in this study, the inferred throat radii span from approximately 5 µm (voxel size) down to approximately 0.23 µm. For simplicity, the five drainage steps are grouped into three throat-size subregion bins, referred to hereafter as Large [5 to 1.54 µm], Medium [1.54 to 0.87 µm], and Small [0.87 to 0.23 µm] subregions, corresponding to sub-resolved voxels that exhibit more than 50% saturation change between two consecutive Pc steps. These subregions spatial maps form the basis for tracking saturation evolution during the subsequent imbibition stage. Fig. *17* illustrates the spatial distribution of the three throat-size regions masks for a representative slice from the top half of the mini-plug. The throat-size bins are not equally represented in terms of pore volume (porosities for subregion are as follows: 14.1 p.u for Large, 3.4 p.u for Medium and 1.8 p.u for Small): the Large subregion dominates the unresolved porosity, a point that becomes important when interpreting imbibition behavior. We note that the sum of subregion porosities does not equal the total unresolved porosity, because not all unresolved voxels are assigned to a subregion bin. Voxels exhibiting slow, gradual drainage across multiple steps (indicative of broad throat-size distributions), as well as weakly connected or minimally drained voxels, are deliberately excluded. This ensures that each subregion bin retains only voxels with a sufficiently narrow throat-size distribution, for which saturation evolution can be reliably linked to a characteristic radii range.

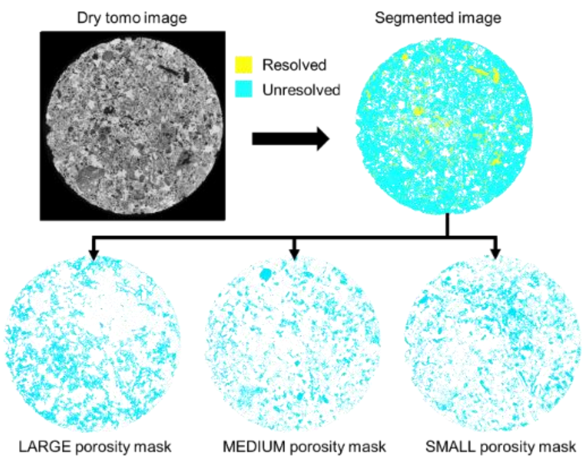

Fig. 17. Spatial distribution of unresolved throat-size regions (large, medium, small) identified from the primary drainage sequence for a representative transverse slice from the top half of the mini-plug.

4.3.2 Unresolved porosity: saturation tracking during imbibition

Once the throat-size subregions bins are defined from the drainage analysis, their saturation evolution can be followed independently throughout the imbibition sequence by overlaying the corresponding subregion masks onto each imbibition Pc step image. For each subregion (Large, Medium or Small) the normalized saturation “µSat” is evaluated at each imbibition Pc step. µSat is the brine volume of a subregion divided by the pore volume of the given subregion. Comparing subregion normalized saturation profiles help determine “where does the brine prefer to go amongst the different unresolved voxel subregions?”. This is fundamentally different from the global water saturation Sw, which is the brine volume divided by the total pore volume of the sample. Two pore-size subregions can exhibit similar µSat values while contributing very differently to the overall Sw, simply because their pore volumes differ. For the purpose of interpreting wettability behavior, µSat is therefore the more appropriate metric, as it reflects the intrinsic affinity of each subregion for brine independently of how much pore volume that subregion bin represents.

Fig. *18* presents the µSat profiles along the sample length for each pore-size bin across the imbibition Pc steps. Two regimes are clearly distinguished: spontaneous imbibition (Pc ≥ −0.035 bar) and forced imbibition (Pc < −0.035 bar). During spontaneous imbibition, brine is not actively forced into the sample; any oil displacement is driven purely by capillary forces and therefore occurs preferentially within water-wet pores. The µSat recorded at these steps therefore represents a minimum estimate of the water-wet pore fraction within each bin, since complex pore connectivity and limited equilibration time at each step may prevent full spontaneous invasion of all water-wet pores. Conversely, during forced imbibition, brine is pushed under applied pressure into pores where capillary entry pressure resists invasion predominantly oil-wet pores.

At the transition (Pc = −0.035 bar) between spontaneous and forced steps, average µSat values show a clear pore-size dependence: 20.0% for Large bin, 17.9% for Medium bin, and 31.1% for Small bin. The markedly higher µSat observed in the Small bin reflects a stronger preferential brine invasion response during spontaneous imbibition relative to the Large and Medium subregions. Notably, the Large and Medium bins exhibit similar µSat proportions at this stage, while the Small pore bin shows a higher value, an observation that warrants further investigation to understand whether this reflects differences in wettability alteration, pore connectivity, or a combination of both. This kind of information is very important as it allows us to assess a minimum proportion of the pore space that remains water-wet after ageing.

During forced imbibition, additional brine invasion is progressively observed across all subregion bins as applied pressure increases. The first forced step (−0.38 bar) primarily affects the large bin, consistent with pressure-assisted brine invasion of pores that resisted spontaneous entry. At −0.7 bar, µSat increases across all bins, although the response of the medium bin remains comparatively limited. This limited response in the medium bin could reflect preferential oil trapping through snap-off or bypassing mechanisms associated with their pore geometry, connectivity and/or wettability. At the final forced step (−1.5 bars), µSat reaches its maximum across all pore-size bins, reflecting progressive brine invasion under increasing applied pressure. Taken together, these observations reveal throat-size-dependent saturation behavior providing physical evidence of wettability heterogeneity in this complex carbonate. Rather than providing definitive quantitative wettability characterization for this specific case, this analysis is intended to illustrate the kind of interpretation framework that the dual porous plate experiment enables: by discriminating throat-size subregions within the unresolved porosity and tracking their saturation evolution independently throughout the full Pc cycle, physically meaningful observations about fluid preference and invasion sequence can be extracted from a domain that is otherwise inaccessible.

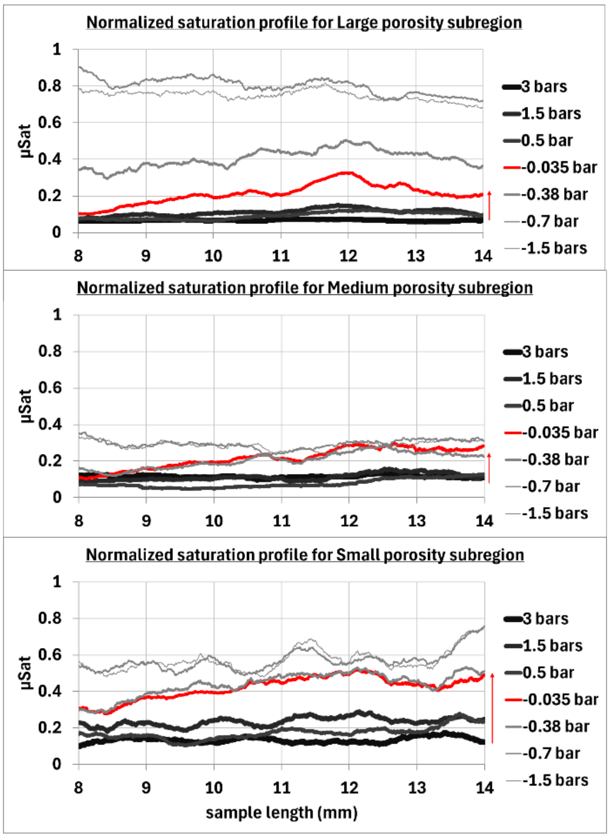

Fig. 18. Normalized brine saturation (µSat) profiles along the sample length for the Large, Medium, and Small unresolved pore subregions at successive imbibition capillary pressure steps. Spontaneous imbibition (positive Pc) shows a stronger response in Small subregion, while forced imbibition (negative Pc) promotes brine invasion across all subregions. The transition between spontaneous and forced imbibition steps (Pc = −0.035 bar) is highlighted in red

Refining this interpretation framework (including sensitivity to experimental conditions, sample heterogeneity, and classification parameters) to be more general will require additional experiments. But the results presented here demonstrate its potential as a tool for informing wettability inputs in pore network modelling of complex rocks alike carbonate reservoirs.

5 Conclusions

This paper introduces and validates a dual-wetting porous-plate system designed to measure, on a single mini-plug and under unchanged boundary conditions, the full drainage - imbibition capillary pressure cycle together with key endpoint permeabilities. The X-ray transparent cell enables systematic 3D saturation monitoring at each imposed capillary-pressure step, thereby extending DRP experimental capabilities to complex rocks in which a large fraction of the porosity remains unresolved by micro-CT. Application to a ~20 mD reservoir carbonate demonstrates (i) an excellent agreement between porous-plate primary drainage results and the SCAL-derived reference Pc function, and (ii) a consistent imbibition behaviour in the most homogeneous part of the mini-plug, supporting the proof of concept and the relevance of the proposed protocol, including controlled ageing without dismantling the setup. Beyond bulk comparisons, the stepwise imaging provides a physically grounded framework to discriminate unresolved throat-size subregions during drainage and to track their pore-size-dependent response during imbibition, evidencing wettability heterogeneity that would otherwise be inaccessible.

The next step would be to formalize the interpretation workflow so that these observations can be translated into robust wettability inputs for pore-network modelling and DRP Kr predictions on complex rocks.

Resolving this experimental workflow's connection with multi-scale imaging could then be the missing link for scaling up DRP modelling to all reservoir types, accelerate development decision making by providing faster, cheaper and reliable reservoir flow properties to reservoir engineers, and reduce reservoir simulation uncertainty by generating more data.

Although this set-up fits perfectly DRP purposes, it also could be applied to SCAL workflows, limiting sample handling risks and experimental artifacts. Full capillary pressure cycle could be monitored at least with effluent production coupled with some end-points permeability measurements.

Acknowledgements

The authors would like to thank TotalEnergies management for the authorization to publish this work.

References

1. Regaieg M., Nono F., Farhana Faisal, T., Rivenq R. Large Pore Network simulations coupled with innovative wettability anchoring experiment to predict relative permeability of a mixed-wet rock. Transport in Porous Media, 147, 495–517 (2023).

2. Regaieg M., Farhana Faisal, T., Nono F., Pairoys F., Fernandes V. and Caubit C. Prediction of relative permeability and fast wettability assessment using Digital Rock Physics: An operational study on a Reservoir Sandstone. SCA2023-26, (2023).

3. Farhana Faisal, T., Nono F., Regaieg M., Brugidou R., Fischer F. and Caubit C. Variation of wettability across different lithotypes in a reservoir and its impact on Digital Rock Physics pore scale simulations. SCA2024-1030, (2024).

4. Lin Q., Al-khulaifi Y., Bijeljic B., and Blunt M.J., Quantification of sub-resolution porosity in carbonate

rocks by applying high-salinity contrast brine using Xray microtomography differential imaging', Advances in Water Resources. 96, (2016).

5. Nono F., Farhana Faisal, T., Fischer F., Pairoys F., Regaieg M. and Caubit C. Pore scale investigation of dopants impact on wettability alteration. SCA2024-1025, (2024).

6. Lenormand R., Eisenzimmer A., and Delaplace P. (1995): "Improvements of the Semi-dynamic Method for Capillary Pressure Measurements." SCA 9531 presented during the International Symposium of the Society of Core Analysts, San Francisco, CA (Sept. 12-14).

7. Longeron, D., Wibeke, L. H., Svein, M. S. Water-oil capillary pressure and wettability measurements using micropore membrane technique. Paper SPE 30006 Presented at the International Meeting on Petroleum Engineering, Beijing, China, 14-17 November 1995.

8. Fleury M., Doevle M., and Longeron D.G., 1997, Full Imbibition Capillary Pressure Measurements on Preserved Samples Using the Micropore Membrane Technique, Paper SCA-9716, presented at the SCA International Symposium, Calgary, Alberta, Canada, 8–10 September.

9. Fernandes V., Caubit C., Nicot B., Pairoys F., Bertin H., Lachaud J., 'Hybrid technique for setting initial watersaturation on core samples', International Symposium of Core Analysts, Austin, Texas, [2022] (SCA2022-23).

10. Lewis M. G., Sharma M. M., Dunlap H. F. and Dorfman M. H., "Techniques for Measuring the Electrical Properties of Sandstone Cores", SPE 18178, 63rd Annual Tech. Conf. and Exh. of the SPE held in Houston, TX, (Oct. 2-5 1988).

11. F. Nono, P. Moonen, H. Berthet and R. Rivenq, 'Multiphase flow imaging through X-ray microtomography: Reconsideration of capillary end effects and boundary conditions', International Symposium of Core Analysts, Pau, France [2019] (SCA2019-019).

12. Raeini A.Q., Bijeljic B., Blunt M.J., Generalized network modeling: Network extraction as a coarse-scale discretization of the void space of porous media. Phys. Rev. E2017;96(1):13312.

13. Puyou, G., N'Guyen M., Savin S., Cxbox: An Innovative Tool for Fluid Dynamic Quantification during Corefloods, SCA2017-037,2017.